Chapter 5

Ultrashort Laser Pulses Machining

Ricardo Elgul Samad, Leandro Matiolli Machado,
Nilson Dias Vieira Junior and Wagner de Rossi

Additional information is available at the end of the chapter

http://dx.doi.org/10.5772/46235

1. Introduction

Over the past several years, the necessity for micromachining technologies has been growing from scientific research to industry. Segments from medical appliances, microelectronics and the automotive world demand a great variety of applications such as micromotors, microfluidic circuits, MEMS (Micro Electrical Mechanical System), medical devices, electronic tooling, particle filters, micromolds and microvalves, among others [1]. This massive growth in the micromachining segment demands a variety of new micromachining methods.

Techniques to machine the surface of materials are continually being improved. Recently, mechanical micromachining with accurate positioning systems and very small drills were used to trim out materials, covering the range from some millimeters down to a few tens of nanometers [2]. A similar technique that also applies direct micromachining and requires a highly accurate positioning system but no contact, is Electron-Discharge Micromachining (EDM), in which material is removed by an electrode guided along the desired path, very close to the surface of a conducting material submerged in a dielectric fluid; a spark is established between the electrode and the material being processed, removing matter by melting and evaporation [3, 4], with micrometric resolution. Similarly to EDM, the Focused Ion Beam (FIB) technique scans an ion beam, with spot sizes ranging from 10 to 500 nm, over a specimen, etching the material [5]. Additionally to etching, this technique can be used to build new structures by localized deposition using the ion beam-induced decomposition of an organo-metallic gas [6]. Examples of the use of a FIB system are the milling of angled cuts into the suspension ligaments of MEMS accelerometers, and the milling of large depth-to-width aspect ratios tracks to make photonic band gap lattices in $As_{40}S_{60}$ [5, 7]. A disadvantage of this technique is that it does not allow batch production due to the small amount of material removed during machining.

Photolithography, a technique that is available for integrated circuits fabrication since the 1970's, has been improved, and nowadays is used to create structures ranging from micrometers, as in the case of MEMS devices, down to tens of nanometers for integrated circuits [8]. This technique selectively removes material from thin films (nitride/oxide /polysilicon) deposited on silicon substrates, and also from the bulk of the substrate [9]. The process consists in using UV light and optical projection to transfer a pattern from a mask to a light sensitive material (photoresist) film pre-deposited on the substrate surface, selectively curing it. The non-cured photoresist is then removed by a developer, and the substrate exposed portions are etched either by a liquid (wet etching) or by a plasma (dry etching). The repetition of many cycles of photoresist deposition and etch can create complex structures, in a process known as *Surface Micromachining*. Different patterns of polycrystalline silicon can be selectively etched and are used as sacrificial layers to create suspended parts attached to the substrate, building 3D structures on the substrate surface [10]. This process enables the creation of structures such as accelerometers [11] and neural probe arrays [12]. When the etching removes a large quantity of material from the bulk of the substrate, the process is known as *Bulk Micromachining* [9], and is used to create devices such as piezoresistive sensors [13]. Photolithography allows batch production, but it is considered the most indirect method, since material is not removed by a tool.

Although largely used, the described techniques have some disadvantages, such as tool wearing (mechanical micromachining and EDM), high complexity (photolithography) and necessity of processing in vacuum (FIB). Besides, when machining different materials, the etching rates can strongly depend on the material and the tool, and the processing parameters, or even the tool, have to be changed. Additionally, the technique can be restricted to a specific material class, such as metals in the EDM case. Other limitations include the small etching speed in the techniques that require precise positioning (mechanical machining, EDM, FIB), preventing batch processing, and the high complexity of the photolithography, which does not allow fast prototyping. In view of those limitations, the ultrashort pulse laser emerges as a valuable tool for micromachining.

Just a few years after the laser invention, it was already being used as a tool to ablate [14] and machine [15] a wide variety of materials, including metals [16], dielectrics [17], semiconductors [18], composites [19] and biological tissues [20]. At that time, the machining was based on thermal processes arising from the material heating by the laser [21], and the ablation occurred as a consequence of melting and vaporization resulting from phase transitions due to the heat deposited into the material being processed [22, 23].

When machining with laser pulses, the laser beam is focused on the material being processed, the light is absorbed and the material undergoes a physical change around the absorption region. The dimensions of the structures that can be machined depend, on a first approximation, on the focused beam diameter. A diffraction limited TEM_{00} Gaussian beam [24] can be focused to diameters close to the laser wavelength, ranging from a hundred nanometers (Excimer UV lasers) to tens of microns (CO_2 lasers). Nevertheless, even with the smallest attainable laser spot on the material surface, the interaction region follows the heat diffusion volume guided by the process dynamics. For long pulses, which last more

than the typical period of lattice vibration (around tens of picoseconds), the dynamics of the laser-matter interaction depends on the laser parameters (wavelength, pulse energy, repetition rate) and on the physical characteristics (absorption, heat capacity, thermal conductivity) of the material being machined. In this long pulse regime, the machining process is a consequence of heating (that results in melting, evaporation, sublimation), depending on the energy absorbed per unit of time and volume, and how it flows inside the material. When the laser radiation is absorbed, the material is heated and thermodynamic processes are responsible for heat diffusion and phase transformations. As the pulse duration shortens, higher intensities are faster achieved, the spatial heat propagation is decreased and phase transformations that lead to material removal occur more efficiently; in this regime, the ablation threshold decreases with the square root of the pulse duration, demonstrating that the ablation is a thermal process [25]. The excess heat that is not used to jettison material flows into the surroundings increasing its temperature, and eventually creating a Heat Affected Zone (HAZ), in which phase transitions modify the material properties, usually in a detrimental way. As a consequence, smaller structures require shorter pulses to be etched, which also produce a reduced HAZ. Nevertheless, although microsecond to sub-nanosecond laser pulses generates intensities high enough to machine metals, semiconductors and even some transparent dielectrics, the heat conduction expands the affected region far beyond the focused beam diameter, creates a large HAZ, and can also generate structures several times bigger than the wavelength used. Collateral effects from heat, like burr, debris and molten material, spread the interaction area limiting the machining precision. Additionally, albeit the high intensities attainable in this temporal regime allow the etching of transparent materials such as sapphire and silica, large amounts of energy are necessary to reach the ablation threshold, resulting in thermal stresses and damages such as chipping and micro-cracking [26, 27]. To handle these problems, different wavelengths are needed for efficient absorption by different materials. For dielectrics, lasers with wavelengths in the UV range are used for better absorption; some glasses have greater absorption in the far infrared [28], hence CO_2 lasers are often employed.

Femtosecond (10^{-15} s) pulses come up as a new possibility for micromachining with some advantages over longer pulses. The machining performed by these ultrashort pulses relies on their very brief duration, which is shorter than the thermal vibration period of the lattice. This small duration minimizes the energy transfer to the material, resulting in an almost nonthermal etching that minimizes the HAZ and preserves the properties of the surrounding material. Also, the ultrashort pulses duration creates very elevated intensities that promote a highly nonlinear interaction with matter, resulting in extremely localized ablations that can etch the material with nanometric precision, allowing the fabrication of very precise, minute structures. Additionally, ultrashort pulses promote a non-selective ablation regarding the material class (dielectric, metallic, etc.), allowing the machining of all kinds of materials with the same laser. The ability of ultrashort pulses to machine any material, even transparent ones, without changing the laser wavelength and the recent availability of relatively cheap, stable, high average power systems that increase the processing speed, are making these pulses very versatile tools to process materials for many high technology applications and devices. Also, in this temporal scale heat diffusion is

minimized, and, with the adequate laser parameters, heat effects can be completely eliminated. Furthermore, is worth mentioning that, although it is not strictly a micromachining technique, the creation of micro and nanostructures is possible by the nonlinear interaction of the ultrashort pulses with a liquid solution. In this technique an ultrashort pulses beam is focused, through an optical a microscope optics, into the liquid solution containing a photosensitive polymer [29] or a photon induced reduction composite material [30]; the multiphotonic absorption that happens at the beam focal region promotes the highly localized solidification of the solution, allowing the manufacture of micro and nanometric structures.

The disadvantages in micromachining with femtosecond pulses comes from the high degree of precision demanded, with consequent necessity of tight focusing that imposes very accurate and expensive 3-axes positioning systems. Also, the low average powers that prevented high batch production are being overcome by modern systems with dozens of watts, allowing increased throughputs.

The invention, in the second half of the 1980's, of the Chirped Pulse Amplification Technique [31, 32], the KLM Ti:Sapphire laser [33], and the diode pumped solid state lasers [34] disseminated the use of microjoule-millijoule (μJ-mJ) ultrashort pulses to many laboratories around the world. The widespread availability of these systems in the decades of 1990-2000, resulted in the emergence of many new applications, including the machining by ultrashort pulses. The most used ultrashort pulse lasers nowadays for machining are Ti:Sapphire and Yb:fiber. The Ti:Sapphire systems can deliver pulses as short as a few tens of femtoseconds, centered at 800 nm, with mJ level energies, and repetition rates up to a few kHz; the Ytterbium based lasers generate pulses centered around 1030 nm lasting hundreds of femtoseconds, and, although limited in energy to the μJ range, operate at tens of MHz repetition rates, increasing its machining speed. Recent developments in laser technology design offer high average power systems [35], which in conjunction with beam conforming devices [36] and high speed scanning systems enable the use of ultrashort pulses machining in batch production, without limiting its fast prototyping capabilities.

2. Ablation by ultrashort laser pulses

The typical characteristics of ultrashort pulses for ablation of solids are energies in the range from tens to hundreds of microjoules, pulse widths around 100 fs and focalization to 20 μm radius spot sizes, generating intensities in the range 10^{12}-10^{14} W/cm^2.

When an ultrashort pulse impinges on a solid, the fact that its duration is shorter than the lattice ions vibrational period means that most of the pulse energy will be transferred to the material electrons, heating them. The majority of the electronic thermal energy will be carried away with the ablated material, and the small remaining portion will be added to the energy directly coupled into the ions, heating the lattice, with the possibility of creating a small HAZ. The control of the irradiation conditions can reduce this HAZ to almost zero.

2.1. Ablation physical mechanisms

The underlying mechanism for ultrashort pulses ablation is almost the same for all material classes (metals, semiconductors, dielectrics, polymers, etc.): when the pulse impinges on the material surface, seed electrons are accelerated by the pulse electrical field into a quivering motion, and either generate free electrons in the conduction band by collisions in an exponential avalanche process [37, 38], or are ejected from the surface due to the acquired kinetic energy [39]. The ejection process has a high occurrence probability on the 100 nm surface layer for electrons that acquired a few eV of kinetic energy, and leaves a charge imbalance that can produce a Coulomb explosion [39-41] of the lattice ions after the pulse. Simultaneously to the surface electrons ejection, the avalanche process occurs in deeper layers in the material, increasing the free electrons density and temperature, while the lattice is kept at a lower temperature (two-temperatures model [42, 43]); if the pulse energy and intensity are high enough, the free electrons density reaches a critical value (around 10^{21} cm^{-3} [38, 44]), and then the electrons transfer its energy to the surrounding ions. This relaxation quickly heats the neighboring lattice above its vaporization temperature, creating an unstable phase that undergoes a violent adiabatic expansion (phase explosion) [45-47], which removes material from the surface, carrying most of the thermal energy with it. Also, spallation [47] and fragmentation [45] can occur, although those are not dominant effects. The energy that is not taken away flows to the lattice, heating it. The dominating mechanism will depend on the pulse characteristics (energy, duration) and material.

For metals, the seed electrons are the conduction band free electrons. For the other materials, the pulse leading edge excites electrons from the valence band either by multiphoton ionization [25, 48] or tunneling induced by the laser field [49, 50]. Once the free electrons are present, a metallization occurs, and the electrons heating evolves deterministically in time [38, 50] in almost the same way in all materials [51].

Depending pulse energy, two ablation domains can be identified: the low and high fluence ones. In nonmetals, these regimes are defined by the dominant ablation mechanism: in the low fluence regime the Coulomb explosion predominates [41], while the phase explosion prevails for the high fluence ablation. In metals, Coulomb explosion does not occur because, at the intensities used in machining, the surface charge accumulation is effectively quenched [40] by the electronic mobility, suppressing the positive ions explosion. The electric field needed to promote positive charge accumulation in metals (~10^{10} V/m) demands intensities around 10^{18} W/cm^2 [52], pushing the Coulomb explosion threshold way above the phase explosion one. In metals, the low and high fluence regimes occur when the HAZ is shorter or longer than the optical absorption depth (Beer´s Law [53]), respectively. The regimes threshold can be predicted using the two temperatures model [42, 43] that describes the electronic heating, diffusion and lattice heating.

For all material classes, the main difference between the two ablation regimes is that in the high fluence there will be fusion in the interaction region, and the remaining material can cool down to an amorphous or polycrystalline phase, whose physical characteristics (mechanical, optical, etc.) can differ from the starting material ones [54]. Also, the HAZ will be bigger in the high fluence regime.

Since, by the mechanisms explained, the ultrashort pulses ablation process depends primarily on the electrons answer to the laser field excitation and not on the thermodynamic properties that arise as a consequence of the atomic lattice, the ablation threshold does not show a square root dependence on the pulse duration [25], as in thermal ablation processes; additionally, the ablation by ultrashort pulses has a nonselective character, and the only parameter that has to be known to etch a material is its ablation threshold fluence, F_{th}. As a general rule, since in nonmetals a portion of the pulse energy is used to create free electrons, these material usually present higher ablation thresholds than metals for the same laser conditions. Also, a single material can present two values for the ablation threshold, one for low and other for high fluence, as can be seen in Figure 1, and they have to be known and taken into account when machining the material.

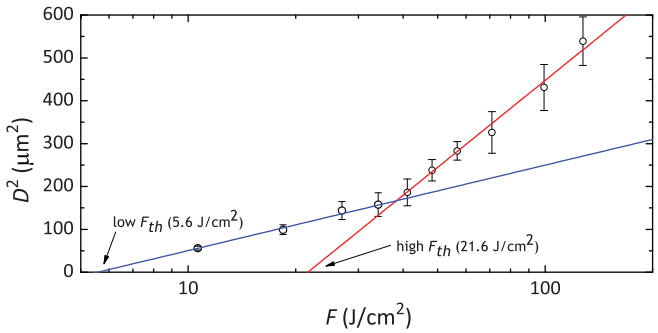

Figure 1. Diameter squared of the region ablated by ultrashort pulses on the surface of Sapphire as a function of the pulse fluence, for single-shot 100 fs pulses [55]. The ablation threshold fluence is given by the fluence at which the ablated diameter is zero, obtained from the fit by equation (1) [56]. The low and high fluence regimes can be clearly identified by two different slopes on the data points.

2.2. Ablation threshold determination

The determination of a given material ablation threshold fluence by ultrashort pulses is usually done using the "zero damage" method, introduced by Liu in 1982 [56]. This method consists in using a TEM_{00} Gaussian beam to ablate the material at various positions in the sample surface, using different pulse energies. Then the diameters of the ablated craters, D, are measured and their square values are plotted as a function of the pulse fluence, F, as show in Figure 1. The data is then fitted by:

$$D^2 = 2w^2 \ln\left(\frac{F}{F_{th}}\right), \tag{1}$$

where w is the beam spot size at the sample surface and F_{th} is the ablation threshold fluence, at which the ablated crater diameter is zero. To execute this measurement, the beam propagation parameters have to be known to calculate its spot size and fluence at the sample surface, and many measurements must be done. Experimentally, this method is

demanding because it requires the precise knowledge and stabilization of the beam parameters, a good sample positioning system to maintain the beam spot size constant at the sample surface for all the measurements, and since it can last a long time, up to hours, it is prone to be affected by laser instabilities. Additionally, frequently the use of an electron or atomic force microscope is needed to determine the crater diameter for fluences close to the threshold, at which the damage size is close to zero and is difficult to be measured.

A few years ago we introduced the Diagonal Scan (D-Scan) technique [57, 58], an alternative and simple method to measure the ablation threshold for ultrashort pulses. The method consists in moving a sample longitudinally and transversely (z and y directions in Figure 2a) across the beamwaist of a focused beam, from a position before the beamwaist, where there is no ablation, to a position after the ablation stops. In this way, a symmetrical profile with two lobes, as the one shown in Figure 2b, will be etched on the sample surface. If the etched profile does not present two lobes, the measurement has to be repeated with a higher pulse energy or with a tighter focusing lens [57].

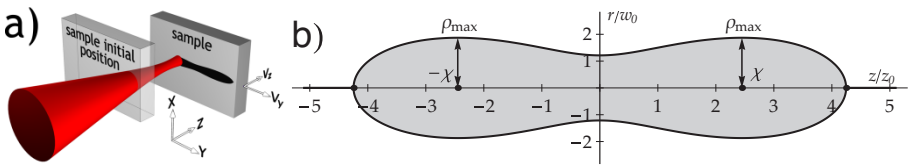

Figure 2. a) Scheme of the D-Scan method. b) profile etched on the sample surface by the diagonal movement across the beam waist position.

It can be shown [57] that the sample ablation threshold fluence is given by:

$$F_{th} = \frac{1}{e\pi}\frac{E_0}{\rho_{\max}^2} \cong 0.117\frac{E_0}{\rho_{\max}^2}, \tag{2}$$

where E_0 is the pulse energy and ρ_{max} is the half maximum transversal dimension of the profile etched.

The determination of the ablation threshold involves knowing the pulse energy and the measurement of the profile maximum transversal dimension (typically a few tens of microns), which can be done in an optical microscope, and the use of equation (2). Compared to the "zero damage" method, the D-Scan is easier to be experimentally performed once it demands only one scan that can be done in a few seconds and a geometrical measurement, replacing a series of measurements that can last a long time, the knowledge of the laser spot size at the sample, and a fitting.

2.3. Ablation by many pulses and incubation effects determination

In a given material, the ultrashort pulses ablation threshold can depend on the presence of defects, dopants, impurities, excitons, etc. [59, 60], which either create intermediate levels in the bandgap or modify the local electronic density. As a consequence, seed and free

electrons are created more easily than in the ideal material, and the ablation requires less energy to occur, lowering the ablation threshold value.

The defects can either be intrinsic to the material, or externally originated, such as color centers created by ultrashort pulses [61]. In this case, when etching solids with superimposing pulses, modifications are induced in the portions that are irradiated but not ablated, lowering these regions F_{th} for subsequent pulses due to defects accretion. The following pulses experience a decreasing F_{th} until the defects density saturates and the ablation threshold reaches a constant value. These cumulative phenomena are known as incubation effects [62-64], and the ablation threshold fluence modification caused by them must be taken into account when machining a material.

A few models were proposed by different authors to describe the incubation mechanisms. One of those is the probabilistic defect accumulation model [62] that, although widely used for different material classes [65-67], does not predict the ablation threshold saturation; other is the exponential defect accumulation model, in which the lowering of the ablation threshold increases the defect creation probability for the next pulse, until the defects saturation is reached and a constant value of F_{th} for the superposition of many pulses is established [59, 60, 63]. In this exponential model, the ablation threshold for the superposition of N pulses, $F_{th,N}$, can be described by [63]:

$$F_{th,N} = (F_{th,1} - F_{th,\infty})e^{-k(N-1)} + F_{th,\infty}, \tag{3}$$

where $F_{th,1}$ is the single shot ablation threshold fluence and $F_{th,\infty}$ is the saturated ablation threshold, below which there is no defect accumulation. If $F_{th,1}>F_{th,\infty}$, incubation effects are present and the ablation threshold decreases as more pulses hit the material; if $F_{th,1}<F_{th,\infty}$ laser conditioning occurs, and the material becomes progressively more difficult to ablate as the pulse superposition grows. In equation (3), k is the incubation parameter, which characterizes the strength of defects accumulation, and is equal or greater than zero. If k=0 the ablation threshold is constant and do not depend on the pulses superposition. As k grows, fewer pulses are needed to reach the incubation effects saturation.

To quantify the incubation effects for a given material, its ablation threshold is measured for various pulse superpositions, including the single shot case, and then equation (3) is fitted to the data. Usually this is carried out using the "zero damage" method, which produces a graphic like the one show in Figure 1 to determine F_{th} for each superposition, demanding a lot of experimental time and data analysis.

It is possible to use the D-Scan Method to determine the ablation threshold for the superposition of an arbitrary number of pulses, $F_{th,N}$, and for that the pulse superposition N that etches the profile maximum transversal dimension, $2\rho_{max}$, has to be known. To calculate this superposition, we hypothesize that it is given by the sum of the intensities generated at ρ_{max} by all the pulses that hit the sample during a D-Scan, normalized by the intensity generated by the pulse centered at ◎ (Figure 2b). Under these assumptions, and also considering that the longitudinal and transversal translation speeds (v_z and v_y in Figure 2a)

are chosen to etch an elongated profile, it can be shown [68] that the pulses superposition N is given by:

$$N = \vartheta_3\left(0, e^{-\left(\frac{v_y}{f\,\rho_{\max}}\right)^2}\right), \tag{4}$$

where f is the pulses repetition rate and ϑ_3 is the Jacobi Theta Function of the third kind [69]. It can also be shown [68] that, when the transversal speed is low or the pulses repetition rate is high, situation in which a large value of N is expected, equation (4) can be simplified to:

$$N = \sqrt{\pi}\,\frac{f\,\rho_{\max}}{v_y} \approx 1.8\,\frac{f\,\rho_{\max}}{v_y}, \qquad \text{for} \quad \frac{v_y}{f\,\rho_{\max}} \approx 0. \tag{5}$$

Using the previous results, the determination of the ablation threshold for an arbitrary pulses superposition requires performing a D-Scan, then using the experimental values of ρ_{max}, v_y and f in equations (2) and (4) to provide $F_{th,N}$ and N. This is a fast experimental procedure since the D-scan can be done in a few seconds for high values of N (and in a few minutes for small ones), and its repetition for varying values of v_y and f quickly provides the ablation threshold for various superpositions, leading to a prompt determination of the incubation parameter from equation (3).

3. Ultrashort pulses machining main applications

The following sections describe ultrashort pulses machining applications, starting from low energy and fluence ones that produce surface modifications, going to high fluence usages that create 3D structures.

3.1. Low and high fluence regimes

Irradiation of metallic or semiconductor surfaces at fluences near the threshold can results in the formation of the so called "ripples", or "Laser Induced Periodic Structures" (LIPSS), which are regularly aligned, long and periodic structures. Their formation is not yet completely understood and is subject of intense study [70]. Typical periodicity is smaller than the laser wavelength, and for enough number of pulses it can evolve to trenches as deep as 1 μm, meaning an aspect ratio of 10 or more. The spacing and orientation of the ripples seems to depend mainly on the beam properties, as energy, number of shots, polarization and angle of incidence, and then, in principle can be controlled to some extent.

Further surface modifications, however, take place as the number of pulses or their energy increase, and the ripple pattern is broken by the formation of cone-like structures, which present a typical feature size and spacing at the order of few micrometers or even smaller. The shape and size of these structures can be further changed with the increase of fluence and number of superimposed pulses, and the use of an acid atmosphere has also been applied to increase the cones height and sharpness. Figure 3 shows examples of LIPSS and cone like structures produced by low energy ultrashort pulses from a Ti:Sapphire laser.

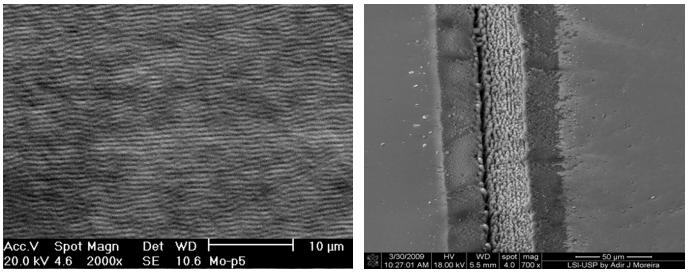

Figure 3. a) Laser Induced Periodic Structures (LIPSS) formed on molybdenum surface. b) Track of cone like structures (white central track) formed on silicon surface.

Up to this point, a minimum amount of material has been ejected from the surface and its topography has not been significantly recessed. To produce substantial depressions it is necessary to further increase the number of shots or the pulse energy. The shape of the created depression resembles the beam intensity profile, and for Gaussian beams the minimum diameter obtained by focusing can be as small as the laser wavelength. If the material and laser conditions allow, heating effects can be neglected, and holes and structures can be directly machined with this size. This is the low fluence ablation regime.

Processing in the low fluence domain can avoid heat accumulation, but the extraction of material is not efficient and only few hundreds of nanometers are etched by each laser pulse. An enormous increase in ejection efficiency is obtained when the fluence is raised to higher values and machining is performed at the high fluence regime. In this regime, heat is accumulated in the affected zone, and several associated phenomena occur. The most important one is the phase explosion, in which the local temperature raises so rapidly that there is not enough time for the material to undergo phase transition. The temperature goes well above the vapor value while the material remains in liquid phase. At this point, a severe explosion happens taking material away from the heated pool.

Machining with high fluence indeed offers high material removal efficiency, but the accumulated heat results in almost the same drawbacks as the ones verified with longer laser pulses that produce thermal ablation. Hence, like in conventional laser processing, this regime leads to debris formation, burr and molten material resolidification on the processed area sidewalls. A HAZ can also appear on the vicinity of the processed volume, causing phase transitions in metals and index of refraction changes in crystals and dielectrics. Due to the very low pulses energy, these effects can extend to a very small region of the produced structure and are irrelevant in many practical cases.

Heating effects also increase the ablated crater size, and the minimum diameter obtained can be far bigger than the focused spot size. On the other hand, low fluence processing can result in affected areas no longer restricted by the diffraction limit. The deterministic character of the laser-material interaction means that ablation will only take place in the portion of the beam cross section in which the intensity is above threshold. Of course this is only possible with a precise control of the laser energy and focus position from shot to shot, and a variation of more than 2% can prevent this possibility.

As already discussed, the complex nature of the ultrashort pulses and matter interaction is responsible for the onset of many different phenomena that depend on the particular characteristics of the laser and the material. The choice of these parameters enables the control of the affected region to produce a rather large amount of diverse structures. Among these possibilities, machining with femtosecond laser pulses can be roughly divided in three great areas: topographic surface modifications, selective ablation of surfaces, and direct writing of microstructures in surfaces and 3D structures in the bulk of transparent materials.

Topographic surface modifications occur when small amounts of material are extracted, resulting in very shallow recesses on the surface, nevertheless affecting its physical and chemical properties. In selective ablation of surfaces, very thin layers of one type of material can be completely etched without affecting the layer bellow it. Direct writing of surface microstructures results in the creation of pre-designed contours and profiles, produced by the relative movement of the laser beam and sample. 3D structures in the bulk of transparent materials are formed when the laser beam passes through the surface of a transparent material and is focused into it, creating complex 3D structures.

3.2. Topographic surface modifications

Nano and micro cone-like structures have been used to trap light and enhance the absorption of reflective surfaces. In particular, this was done by Mei et al. [71] on the surface of silicon with the purpose of using it as an improved sun light absorber. In their experiment, very thin and flexible pieces of silicon were irradiated by femtosecond pulses followed by HF etching. This acid etching enhances the micro spikes sharpness produced by the laser and increases the structure number of reflections, resulting in enlarged light absorption. The irradiation was done in the presence of sulfur hexafluoride (SF_6), which further improved light absorption by creating impurity bands due to sulfur atoms doping during laser irradiation.

Halbwax et al. [72] produced slightly different geometries of such micro structures on n-type silicon doped phosphorus. This was done by varying processing parameters in vacuum. Even using high fluence irradiation, spikes and other structures were formed with size and spacing in the few micrometers range. After boron implantation, these structured surfaces presented an increase of more than 30% in light absorption induced photocurrents, showing its potential for use in photovoltaic cells.

Nano and micro structures have also been used to change physical and chemical properties of titanium and ceramics surfaces in order to improve their biocompatibility for medical implants [73]. This is possible by creating very small structures on their surfaces, enabling, to some extent, the control of cellular growth and adhesion, inhibiting or promoting proliferation of certain types of cells. In this respect, Vorobyev et al. [74], produced several kinds of sub-micrometric structures on pure titanium surfaces by femtosecond laser irradiation. By the use of low and high laser fluences, and varying the number of overlapped laser shots, they produced diverse structures like nanostructured LIPSS, sphere-

like nanoprotrusions and columnar microstructures, whose featured size ranged from few dozens of nanometers to hundreds of micrometers.

The same kind of texturing has also been studied to improve the tribological properties of several materials. This has been specially done on thin films of hard materials such as TiN and diamond-like carbon [75], in which nanostructured LIPPS changed the micro and macro frictional properties and hardness of these materials. Another consequence of the formation of micro arrays as cone-like or pillars, is their interaction with water, keenly increasing the contact angle of the liquid with the surface. By controlling the aspect ratio of these arrays, super-hydrophobic surfaces have been produced [76, 77], creating self-cleaning surfaces and which are also believed to take an important role in cell control processes.

As the presence of micro and nano structures on metal surfaces changes its interaction with light, some research has been done to control the surface reflectivity, and hence the perception of its color [78, 79]. The control of shape, size and spacing of gratings on surfaces is a well-known way to control the reflectivity of light; therefore, ripples formed by nano-structured LIPSS obtained by femtosecond laser irradiation are a natural approach to accomplish such a task. These characteristics can be controlled by handling some process parameters, as fluence, polarization direction, angle of incidence and scanning speed. The final shape comprises self-produced micro/nano gratings maintaining an almost fixed pitch and direction, covering a large area. Besides using LIPSS, color in metals has also been done by directly machining small grooves and arrays of micro-holes in their surfaces. Consequently, structuring metal surfaces in scales from nanometers up to hundreds of micrometers allow the control of the optical properties, from UV to terahertz.

3.3. Selective ablation of surfaces

The ability of ultrashort laser pulses to ablate very thin layers of material can be used to selectively remove coatings overlaid on a substrate. Layers as thin as a few hundreds of nanometers can be removed by each laser shot, and the process can be repeated up to the point where all the unwanted material is removed and the substrate is stricken by the laser beam. This process can be a precise and useful tool in many applications [80-84], as cleaning, restoration of art objects, decontamination and decoating of cutting tools.

The differences in physical properties between coating and substrate determine the feasibility, precision and complexity of the process. If the material to be removed absorbs the laser wavelength and presents a lower ablation threshold than the substrate, then the process is relatively simple and there is no need for feedback control. The pulse fluence is adjusted to be above that of the coating and below that of the substrate; an excess of pulses on the substrate surface will not affect it. On the other hand, if the coating damage threshold is close or lower than the substrate one, then a feedback must control the ablation process to prevent damage to the substrate. This can be accomplished by measuring, in real time, the spectrum of the emitted plasma (LIBS [81]) and observing the evolution of characteristics emissions of the coating and the substrate.

3.4. Direct writing microstructures in surfaces

Regardless of the topographic structures formed on a surface hit by femtosecond pulses, they can be used in a bigger scale to process complex structures previously designed, just like in a milling machine. Tiny holes and channels with high aspect ratios can be produced in almost any kind of material, with very high dimensional resolution, no heat effects, and beautiful cosmetic appearance.

Due to the relative low average power of the femtosecond laser systems, large processed areas or high ablated volumes still present a very low productivity, and are only considered when other methods fail. This happens when tiny structures must be produced on sensitive or transparent materials, when heating effects and dross must be avoided, and when sub-micron lateral size and resolution must be attained.

Although some processes use femtosecond laser assistance to produce sub-micron holes [85], these have also been directly drilled on thin films by precisely controlling the fluence just above the threshold [86]. Gaussian beams tightly focused produce a steep spatial intensity (fluence) distribution which precisely determines the diameter within which the fluence is above the threshold of the material. So the intended diameter of a hole can be achieved by using proper laser fluence and few hundreds nanometers holes can be directly drilled in thin films [87, 88].

Alumina is a very sensitive material that frequently presents cracks, delaminations and striations on the laser processed surface. However, some authors [89, 90] have managed to produce high aspect ratio and low tapered holes in alumina wafers suitable for micro-vias used in micro-electronic circuits. In trepanation mode, high fluences can be used in conjunction with other processing parameters in a way that minimizes heat accumulation and avoid recast molten material, cracks and delamination. Drilling in percussion mode produces smaller diameters, but these are dependent on the laser fluence. Unlike with longer pulses, however, the hole sizes almost do not depend on the number of overlapped pulses, which results in an easier and more precise production. Although percussion drilled holes present more tapered profiles, high aspect ratios can be obtained in relatively thick materials; typical diameters of a few dozens of micrometers are easily done on hundreds of micrometers thick alumina plates.

Structures with complex shapes in almost any kind of material can also be done by cutting and sculpting cavities with femtosecond lasers. The exact knowledge of the phenomena occurring during the laser material interaction allows the production of previously designed shapes in the same way as in a milling machining, with very high precision, but in a much smaller scale. Lateral and vertical accuracies depend on the fluence used and on the aspect ratio figure, but sub-micron or a few micrometers resolution is easily attained. Plates with thicknesses in excess of 0.5 mm have been cut to produce microparts and functional elements used, for instance, in MEMS and other microsystems. Carving into bulk or deposited films can also be done to produce trenches, microchannels and molds with applications in microelectronics, microfluidics and MEMS.

Just like in a milling process, machining with ultrashort laser pulses has been done in complete CAD/CAM systems where not only the toolpath has to be controlled, but also the energy and the number of overlapped pulses. Unlike a real milling tool, the size of a damage produced by a fixed laser focused spot increases as the number of shots accumulates (up to a certain point) on the same spot, and the same occurs by the increase in the pulse energy. Hence, the process control software must be fed with the fundamental parameters governing the interaction of the material with ultrashort pulses.

Although scanning mirrors can be used, the most common femtosecond processing systems use stable and precise 2D or 3D translation stages, with a still beam focused by a short focal length lens. Some cases demand vacuum processing, but generally the machining is performed in regular atmosphere with no shrouding gases. The pulse energy is controlled by a combination of a polarization rotator and an analyzer, and the pulses overlapping is calculated by combining the scanning speed with the laser repetition rate and the focused beam diameter.

As isolated components or as parts of a mechanical microsystem, tiny pieces have been machined in a variety of materials and shapes to an increasing number of new applications, where sensors and actuators for MEMS and microchannels for microfluidics are among the most important examples. Silicon, glasses and several kinds of ceramics, polymers and metals have been used to produce structures for these and other applications.

Silicon is one of the most largely studied materials for ultrafast laser machining, and silicon wafers have been cut and etched by laser to produce micro-molds to be used in a large number of micro electromechanical systems and electronic devices [91, 92].

Many kinds of polymers have also been machined by femtosecond lasers, mainly to produce small channels for rapid prototyping of microfluidic devices, and optical gratings. Suriano et al. [93] determined process protocols for laser machining of some polymers, showing the feasibility to obtain good shapes from some kinds of thermoplastic polymeric materials. Despite good geometrical and cosmetic results, some degradation, probably due the use of high fluences, was observed; physicochemical modifications in the processed area caused some darkening which was explained in terms of oxidation, dehydrogenation or thermal depolymerization.

Microstructured optical fibers were transversally machined to provide access to its core with minimum interference in their optical and guiding properties [94]. Micrometric transversal holes machined through polymeric cladding and glass core enable filling the fiber with fluids to take advantage of their optical properties for uses in sensors and in flexible microfluidic devices. Figure 4 shows an example of a square hole machined on the surface of a hollow fiber to allow gas filling to modify its optical properties.

In the work of Alemohammad et al. [95] a series of micro-grooves were transversally and accurately machined on the cladding of a fiber Bragg grating. This structure increases the transmission sensitivity of the fiber to the index of refraction of the external medium, making these engineered fibers a powerful tool for measurements of temperature and

liquids concentrations. This is a good example of how controlled such machining can be, since it was precisely done (22 μm wide × 32 μm deep grooves with 50 μm pitch) on a thin polymer curved surface without damaging the core beneath it.

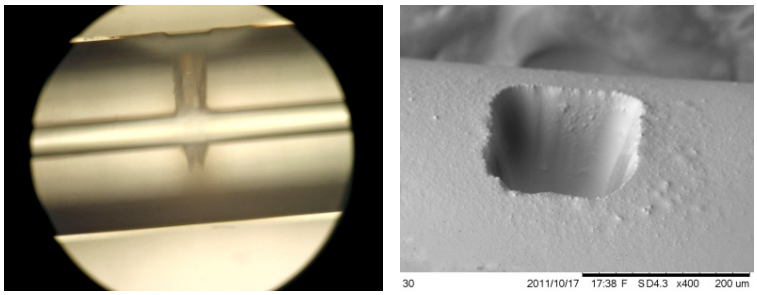

Figure 4. Hole bored in a hollow fiber with ultrashort pulses, using trepanation. a) fiber lateral view optical micrograph, and b) hole entrance view electron micrograph.

Another example of accuracy in laser processing of fibers is the machining of their core end faces [96]. Arrays of sub-micrometric structures boost the signal of a surface enhanced Raman scattering fiber probe, increasing its sensitivity for the detection of many biological and chemical substances. Minuscule cantilevers directly machined in one end of the fiber provided a very sensitive way of movement detection [97].

3.5. Micromachining in metals

Machining metals with ultrashort laser pulses is not as advantageous as machining dielectrics. The presence of free electrons, besides inhibiting Coulomb ablation, widens the heat affected region due to their high mobility. In this sense, the metal thermal properties play a fundamental role in the process characteristics and taking these into account, reproducible, small and accurate structures can still be produced [98].

The control of the pulse duration and wavelength can further improve efficiency and accuracy when machining some metals [99-101]. In a general way, as the pulse shortens (below 1 ps), the finishing improves and the ablation rate increases. Low fluence regime gives the best quality results, but at the same time implies a low ablation rate. Hence, work in this regime is only advantageous with systems offering high repetitions rates at moderate energies [102].

Another approach to increase efficiency is to work in the high fluence regime, where thermal processes, including phase explosion, fully control ablation. In this case, unlike pico or nanosecond pulses, almost all molten material is blown away in the form of nanometric particles, leaving a smooth and clean surface with almost no debris or dross and a negligible HAZ. Indeed, heat can be accumulated also from pulse to pulse as function of the laser repetition rate and thermal properties of the metal. Additionally, for sufficiently high repetition rates, the plume from the previous pulse can also provide shielding that scatters and absorbs pulse energy. Due to this, when processing with high repetition rates, from

hundreds of kilohertz to some megahertz, efficiency and accuracy may vary according to the metal and process characteristics.

There are many examples of machining with femtosecond pulses to produce small devices in metals; some of the most common are microcantilevers [103], coronary stents [104] and pieces of NiTi shape memory alloy [105] used in MEMS. Percussion hole drilling in metals [106, 107] is also another application that is quickly growing. Thicknesses up to 0.5 mm and accuracy of few micrometers are reported in many different metals and applications, most of them without shrouding gas or vacuum, using fundamental wavelengths (800 nm or 1030 nm) and pulsewidths from 100 fs to 800 fs. The parts produced frequently do not need re-work or etching for cleaning and better finishing.

3.6. 3D structures in the bulk of transparent materials

The ablation threshold of the bulk of a transparent medium is considerable higher than of its surface (about twice). Even so, damages forming complex 3D structures can be produced in materials transparent to the wavelength used, by tightly focusing the laser beam below their surfaces. The requirement is to ionize and produce plasma in a volume inside the material, without affecting the surface above. To accomplish this, high numerical apertures (N.A.>0.5) objectives must be used to focus the beam under the surface, in a condition where the fluence is below the threshold on the surface, and at the same time overcomes the volume ablation threshold at the focus. In general, for glasses, nonlinear absorptions are induced for intensities in the range of $1\text{-}5\times10^{13}$ W/cm^2, which can be easily reached by any combination between the main processing parameters (pulse energy and duration, and beam diameter at focus).

For a laser beam with good fundamental spatial mode, the diameter of the focused spot can be close to its wavelength (800 nm for Ti:Sapphire laser, 1 μm for Yb:fiber). Practical temporal pulsewidths range from 30fs to 200fs for Ti:Sapphire and from 200 fs to 400 fs for Yb:fiber. Hence, less than 10 nJ are enough to create damages in the bulk of glasses when using Ti:Sapphire lasers, and this figure increases to 30–160 nJ when using Yb:fiber lasers. Under these conditions, induced absorption occurs in a volume of less than 1μm^3, and a single femtosecond pulse is enough to create damage in the bulk of any transparent material [108]. Within this volume, super-hot dense plasma is formed, creating very strong shock waves that destroy any atomic arrangement, resulting in modified structures or even voids.

The use of UV fs pulses enables the creation of even smaller defects into transparent materials, since its wavelength is shorter than near IR. Furthermore, the higher UV photon energy also increases the probability of multiphoton absorption, decreasing the breakdown intensity threshold. Using this approach, Dubov et al. [109] reported the production of 250 nm periodic nanostructures using 30 nJ, 300 fs laser pulses.

For intensities below the threshold, only nondestructive effects can occur, such as changes in the index of refraction of the material and color centers creation [61]. The presence of these defects produces intermediate levels in the band gap of the dielectric, resulting in incubation effects that usually lower the material damage threshold.

Although not a strict micromachining, permanent modification in the optical index of refraction have been extensively used to create light guiding structures in the bulk of transparent media [110, 111]. The relative movement of the laser beam focus inside the material produces a pathway with cross section and index of refraction contrast suitable to guide light as waveguides embedded in the material bulk. The focus movement can be done in the same direction as the beam propagation, or perpendicular to it. In the first case, the modified region presents a cross section with circular geometry, and in the other this geometry is elliptical. In spite of this disadvantage, the transversal geometry is preferred once the sample and waveguide lengths are not limited by the depth of focus as occurs in the longitudinal method.

The refractive index change depends on the laser parameters and material composition, and is induced by many different mechanisms not yet fully understood. The change can be either positive or negative, depending on the material properties, and is caused mainly by thermal effects, defects creation and material densification. High repetition rates (a few MHz) are generally used, causing heat accumulation with consequent melting and fast cooling in the focal volume scanned by the laser. These rapid phase transitions result in local structural modifications, giving rise to changes in the optical index of refraction that can be over 1%.

Many passive and active guiding structures have been incorporated in devices mainly used in communications and biochemical applications. Couplers, splitters and delay lines are some of the more typical, but more sophisticated structures, as interferometers and diffraction gratings, have been also produced.

Focusing the laser beam in the bulk of a transparent material, just above its damage threshold, causes local structural changes that affect its physical and chemical properties. In the case of sapphire and glasses, their chemical resistance to HF acid and KOH are considerable lowered, reaching a ratio of $1{:}10^4$ for sapphire and $1{:}10^2$ for glasses. This phenomenon has been used to produce hollow channels inside these materials when irradiating with femtosecond laser pulses. After laser irradiation, the material with complex modified 3D structures inside, is etched with a solution of HF acid (or KOH) for up to 48 h to remove the modified material, and results in a hollow structure.

Another approach to make 3D hollow structures inside transparent materials is by focusing the laser beam on the rear surface of a glass sample that is in contact with water [112]. Movements of the focused spot in the vertical direction create a microchannel entering the material's bulk while the water removes the debris formed during irradiation. The process is then continued and complex structures can be produced in all directions.

4. Case studies

The following sections present results obtained in our laboratories regarding the determination of ultrashort pulses ablation threshold and incubation parameters in various materials, and the micromachining in the low and high fluence regimes.

4.1. Silicon ablation threshold measurement

The "zero damage" method was used to determine the ablation threshold for crystalline silicon. For this, 30 μJ maximum energy, 100 fs (FWHM) pulses, centered at 800 nm, at 1 kHz maximum repetition rate, generated by a Ti:Sapphire CPA system (Odin, from Quantronix) were focused on the sample surface by a 38 mm lens. The sample was fixed to a computer controlled translation stage. Many measurements were performed to obtain $D^2 \times F_{th}$ data for different pulses superpositions N, as shown in Figure 5a for N=1. In this graph the low and high fluence ablation regimes are clearly seen, and the fits by equation (1) provide the values 0.32 J/cm² and 8.7 J/cm² for the low and high fluence ablation thresholds, respectively. Crystalline silicon shows a curve $D^2 \times F_{th}$ with the same characteristics seen in dielectrics, as exemplified by the sapphire results shown in Figure 1, with an abrupt slope change when thermal effects start to dominate and the material removal rate sharply increases.

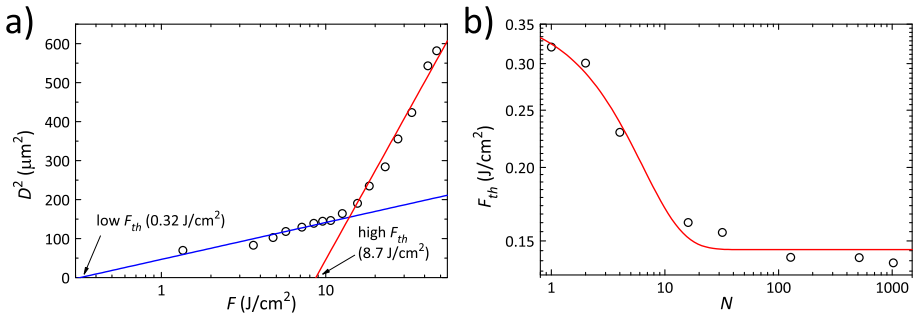

Figure 5. a) Square diameter $D^2 \times F_{th}$ for single pulse ablation (N=1) of silicon; b) Silicon damage threshold as fuction of the pulses superposition.

Figure 5b shows the low fluence ablation threshold measured for different pulses superpositions N, together with a fit by equation (3), which provides $F_{th,1}$=0.32 J/cm², $F_{th,\infty}$=0.15 J/cm² and k=0.22. It can be observed that the defects accumulation is strong in this material, and saturation of the ablation threshold occurs for less than 50 pulses.

4.2. Molybdenum ablation threshold measurement

The "zero damage" method was also used to determine the ablation threshold of metallic molybdenum, repeating the experiment performed with crystalline silicon described in section 4.1. The diameter of the ablated region as a function of the pulse fluence, for the superposition of 4 pulses on the surface of polished molybdenum, is shown in Figure 6a, together with a fit by equation (1), providing F_{th}=0.019 J/cm². This graph shows that the fluence increase does not exhibit an abrupt slope change from the low to the high fluence regime, instead a smooth transition is observed, demonstrating the onset of new processes as the fluence grows.

The ablation threshold dependence on the pulse superposition data, together with a fit by equation (3) is shown on Figure 6b, and, as is the case with dielectrics and semiconductors

(Figure 1 and Figure 5b), it can be seen that the damage threshold decreases as the number of overlapped pulses grows. The values returned by the fit are $F_{th,1}$=0.051 J/cm², $F_{th,\infty}$=0.0136 J/cm² and k=0.84, evidencing that saturation is quickly reached for less than 10 pulses. Nevertheless, more data points around this value would provide a better result.

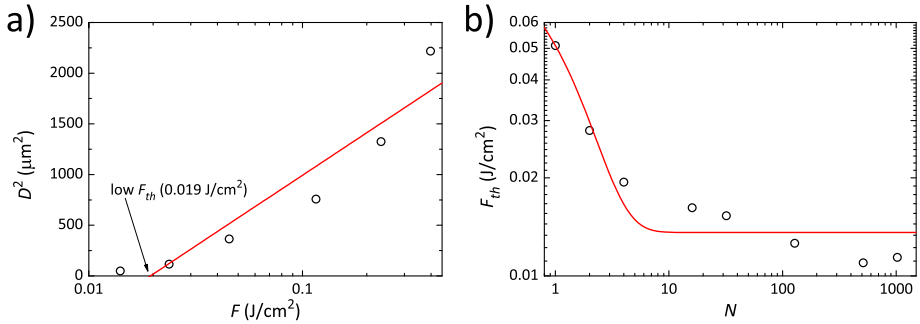

Figure 6. a) Square diameter dependence on the ablation threshold fluence for N=4; b) ablation threshold fluence $F_{th,N}$ as a fuction of the pulses number.

Comparing the single shot fluence ablation thresholds obtained by us for sapphire (5.6 J/cm², Figure 1), silicon (0.32 J/cm², Figure 5a) and molybdenum (0.051 J/cm², Figure 6b), it can be seen that, as the easiness to generate free and seed electrons increase (bandgap decreases), the ablation threshold value drops, as expected by the reasons discussed in section 2.1.

The behavior seen in Figure 6 implies that machining metals with ultrashort pulses is more challenging than machining dielectrics, demanding a better knowledge and control of the process parameters, and sometimes requiring a rework for finishing. The absence of ablation by Coulomb explosion means that always there will be some heat flow to the surrounding area and the conditions of machining must be adjusted to minimize its effects.

4.3. Validation of the D-scan method for ablation threshold and incubation parameter determination

To demonstrate that the D-Scan is a valid method to determine the ablation threshold for an arbitrary pulse superposition, we measured the ablation threshold of BK7 samples by the "zero damage" and D-Scan methods, and compared the results. A Ti:Sapphire CPA system (Femtopower Compact Pro CE-Phase HP/HR, from Femtolasers) was used, continuously generating 100 fs (FWHM) pulses centered at 785 nm with 40 nm of bandwidth (FWHM), at a maximum repetition rate of 4 kHz. The pulses were focused by a 38 mm lens for both methods, and all measurements were performed in air. For the "zero damage" method, the F_{th} was measured for single pulses and for the superposition of 2, 4, 16, 32, 120, 510 and 1020 pulses, and the results, calculated using equation (1), are show as red circles in Figure 7 [68].

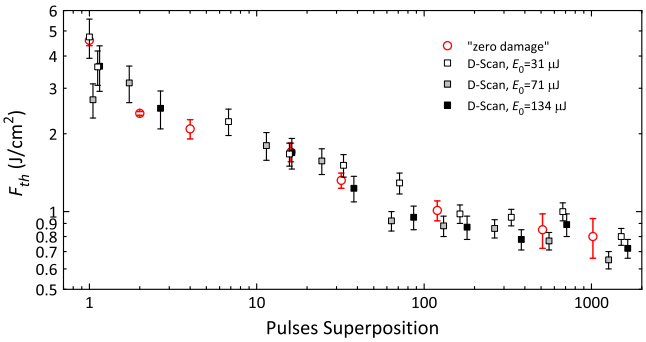

Figure 7. BK7 Ablation threshold measured by the traditional (red circles) and by the D-Scan (squares) method [68]. The good data agreement shows the methods equivalency to determine ablation thresholds in the ultrashort pulses regime.

For the D-Scan measurements, the sample was irradiated by 31, 71 and 134 μJ pulses, at various combinations of repetition rates (50, 100, 500, 1000, 2000 and 4000 Hz) and transversal displacement speeds (6, 12, 25, 50 and 100 mm/min) resulting in superpositions ranging from single pulse to almost 2000 pulses. The Results are show as squares in Figure 7 [68]. This graph shows that the ablation thresholds obtained by both methods agree for superpositions spanning more than 3 orders of magnitude. This implies that the superpositions measured by both methods, although conceptually different (in the "zero damage" the superposition is the number of pulses that completely overlap at the same spot, while for the D-Scan it is given by the sum of the intensity of many pulses spatially apart), are the same, indicating that incubation effects are a linear sum of the intensities that hit a spot. This intensity linear sum effect is also corroborated by the fractionary superpositions that can be observed in Figure 7 D-Scan results for the superposition of less than 10 pulses, which are consistent with the values obtained for integer values of N.

4.4. D-scan technique determination of the incubation parameter of optical materials

The D-Scan method was used in our laboratories to quickly determine the incubation parameter for two common optical materials, sapphire and suprasil glass. The same Ti:Sapphire CPA system described in section 4.3 was used, continuously generating 95 μJ, 25 fs (FWHM) pulses. The beam was focused by a 75 mm lens, and the samples were fixed to a 3-axes computer controlled translation stage that executed the diagonal motion. The measurements were done using various combinations of the pulses repetition rate (100, 500, 1000 and 4000 Hz) and transversal displacement speeds (10, 5, 2.5, 1.25, 1, 0.5, 0.25, 0.2, 0.1, 0.05, 0.04, 0.03, 0.02 and 0.01 mm/s), and it took less than 1 hour to etch more than 35 profiles in each sample. The ρ_{max} value for each profile was measured in micrographs taken in and optical microscope, and the ablation threshold and superposition values for each profile were then calculated using equations (2) and (4). The results are exhibited in Figure 8, and

show that in about 1 hour of laboratory time, it is possible to perform measurements that produce data spanning more than four orders of magnitude of *N*, revealing the dynamics of the defects accumulation until saturation is reached. One of the strengths of the D-Scan technique, which is fast data acquisition, becomes evident when comparing the graphs exhibited in Figure 8 with the ones shown in Figure 5b and Figure 6b: lots of data points are obtained (in a short time), allowing a detailed analysis of the incubation effects, and deciding which model is better to describe them. This kind of analysis is very arduous to be performed with data gathered with the "zero damage" method, due to its complexity that demands a lot of laboratory and data analysis time.

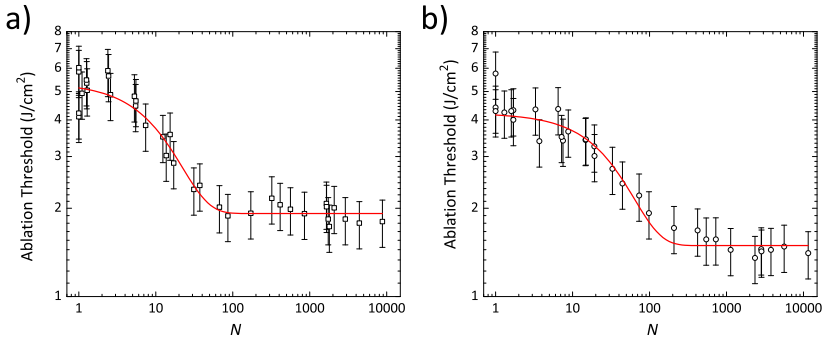

Figure 8. Ablation threshold as a function of the pulse superposition measured using the D-Scan technique for a) suprasil and b) sapphire samples. In each graph, equation (3) is fitted to the data.

To determine the samples ablation thresholds and incubation parameter, equation (3) was fitted to each sample data (red curves on Figure 8), and the parameters obtained are shown in Table 1. The parameters in this table highlight what can be seen in Figure 8: laser created defects have a faster accumulation rate in suprasil (higher k), in which saturation of the ablation threshold is reached for less than 100 pulses, in contrast to sapphire where approximately 500 pulses are needed to saturate F_{th}. Nevertheless, saturation fluence is lower in sapphire, indicating that defects electrons are easier excited in this material.

Sample	$F_{th,1}$ (J/cm²)	$F_{th,\infty}$ (J/cm²)	k
Suprasil	5.1±0.1	1.92±0.05	0.064±0.008
Sapphire	4.2±0.1	1.49±0.04	0.022±0.003

Table 1. Fit parameters for each sample

4.5. Direct micromachining of microchannels in BK7

In direct machining of cavities, multipulse ablation is often needed to remove the necessary amount of material, and incubation effects occur. These effects must be taken into account when establishing the machining parameters to ensure adequate control of the ablation process. Within this context, this section presents a study on BK7 etching, in which this approach was used and produced microchannels with shapes, dimensions, finishing and HAZ complying with the requirements for microfluidic devices [113].

To evaluate the efficacy of the method, two different strategies were used, and in both approaches, several parallel lines were swept by the focused laser spot to create a channel with the desired width. For each scanning, a different lateral offset distance d (Figure 9) was used.

The first strategy, named hard machining, consists in working in the high fluence regime, with a high material removal rate, and low longitudinal displacement speed (large longitudinal pulse superposition N). The second approach, dubbed smooth machining, uses a high displacement speed (small N) and operates in the low fluence regime, removing small amounts of material per pulse. This condition sweeps the surface with a smaller number of shots when compared to the hard machining, making it necessary to repeat the process many times (many sweeping layers) to reach the desired depth [113].

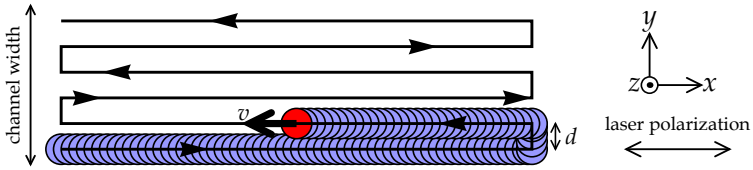

Figure 9. Diagram of the beam path for one etched layer. The beam polarization and scanning direction are parallel to the channel longitudinal axis.

For the hard machining, microchannels were etched with 1 kHz repetition rate, 33 μJ maximum energy pulses, constant scanning speed at 1.6 mm/min chosen to produce a pulses superposition N=500, and varying offsets d for each different channel. These irradiation conditions lead to asymmetric, shallow and irregular channels, as can be seen on the transversal section OCT images shown in Figure 10. In this image, the ablated regions are clearly seen for each track, together with very deep and tapered modified regions below the ablated surface. These regions, which cannot be seen by optical microscopy, are not related to catastrophic damage, and can only be observed by OCT due to changes in the index of refraction caused by nonlinear effects resulting from the pulses high intensity [114, 115].

The subsurface modified regions are a consequence of incubation effects. As the pulses overlap increases, F_{th} is lowered, and a greater fraction of the pulse energy is used to cause more severe effects on the processed material. The large amount of ablated material also produces a skewed wall for each individual track. As consequence, the sloped walls of the machined track reflect the subsequent pulses to the adjacent track that follows it, making the ablated area erratic and unpredictable [113].

In the smooth ablation strategy, the lateral displacement d was changed in each layer to always maintain a fixed overlap of 25% of the created damage diameter, since the size of the

ablated area changes due to incubation processes. In each layer, the total width of the machined track takes into account the many sweeps to keep the lateral overlap constant, spreading the amount of pre-damaged material smoothly and homogeneously. When this is not considered, the deposited energy is more quickly absorbed in places where accumulation of pre-damages is greater, resulting in a non-homogeneous ablation.

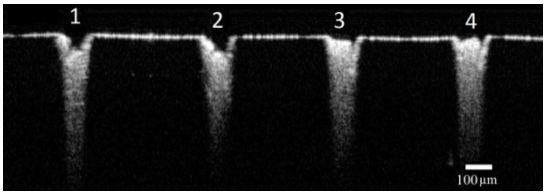

Figure 10. Cross section OCT image of the channels etched by "hard machining". The lateral displacements are d=10, 20, 30 and 40 μm for channels 1 to 4, respectively.

The width D of the ablated track during each sweep depends on the incubation resulting from the *previous* layers etched by N_{n-1} pulses superimposed, and the longitudinal overlap of the *actual* scanning, N_{actual}, where n is the layer number. Within these considerations, the total superposition to calculate D is $N_n=N_{n-1}+N_{actual}$. Thus, D is a function of the beam radius on the machined surface, w, the peak fluence of each pulse, F, and the ablation threshold $F_{th,N}$ for total incubation contribution N, and can be obtained using equation (1) (substituting $F_{th}=F_{th,N}$).

Finally, the value of the longitudinal superposition of the actual scanning, N_{actual}, can be determined by employing equation (4) using the scanning speed v, the repetition rate f and considering that the $\rho_{max}=w$ (beam radius on the sample surface).

A clear improvement in the channels shape occurred when the smooth machining ablation was used, as shown in the OCT image on Figure 11. The channels cross section shows a flat bottom and straight walls, almost perpendicular to the surface. Refractive index modifications below the channels are absent, evidencing that the material properties are preserved in the immediate vicinity of the machined regions.

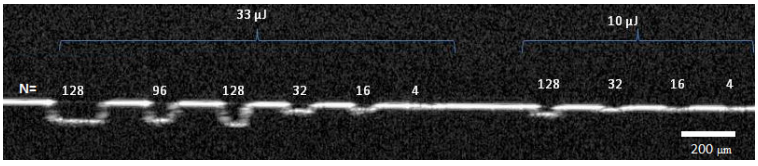

Figure 11. Cross section OCT image of the channels etched by the smoot machining strategy. The total number of overlapped pulses, N, is indicated above each channel. Pulse energies of 10 μJ and 33 μJ were used.

5. Conclusions

In this chapter we presented an overview of micro and nano machining with ultrashort laser pulses. A historical context was provided, the basic physical mechanisms governing the ablation of solids by femtosecond pulses were described, some relevant real-world applications were outlined and experimental results obtained by us were presented. The text references many important and cornerstone works, and the reader who wants to expand his knowledge and have a deeper understanding in this field should start by reading these books, reviews and papers.

The most important parameters to machine a material with ultrashort pulses are its ablation threshold fluence and incubation parameter. Two techniques to determine these parameters were described, the traditional "zero damage" and the D-Scan methods. Experimental results obtained by both techniques were presented, showing that the methods are equivalent, and both can be used to determine these parameters. Nevertheless, we recommend the use of the D-Scan technique because it is experimentally simpler, provides quick results, and the material modifications caused by it are closer to the final machining results once it is executed in a moving sample.

Author details

Ricardo Elgul Samad, Leandro Matiolli Machado,
Nilson Dias Vieira Junior and Wagner de Rossi
Instituto de Pesquisas Energéticas e Nucleares – IPEN-CNEN/SP, Brazil

6. References

[1] Gad-el-Hak M (2006) MEMS : introduction and fundamentals : the MEMS handbook. Boca Raton: CRC Press/Taylor & Francis. p.

[2] Dornfeld D, Min S, Takeuchi Y (2006) Recent Advances in Mechanical Micromachining. CIRP Ann.-Manuf. Techn. 55: 745-768.

[3] Pradhan B, Masanta M, Sarkar B, Bhattacharyya B (2009) Investigation of electro-discharge micro-machining of titanium super alloy. Int. J. Adv. Manuf. Tech. 41: 1094-1106.

[4] Kaminski P C, Capuano M N (2003) Micro hole machining by conventional penetration electrical discharge machine. Int. J. Mach. Tool Manu. 43: 1143-1149.

[5] Langford R M, Dale G, Hopkins P J, Ewen P J S, Petford-Long A K (2002) Focused ion beam micromachining of three-dimensional structures and three-dimensional reconstruction to assess their shape. J. Micromech. Microeng. 12: 111-114.

[6] Malek C K, Hartley F T, Neogi J (2003) Fast prototyping of high-aspect ratio, high-resolution X-ray masks by gas-assisted focused ion beam. Microsyst. Technol. 9: 409-412.

[7] Dale G, Langford R M, Ewen P J S, Reeves C M (2000) Fabrication of photonic band gap structures in $As_{40}S_{60}$ by focused ion beam milling. J. Non-Cryst. Sol. 266–269, Part 2: 913-918.
[8] Chou S Y, Krauss P R, Renstrom P J (1996) Imprint lithography with 25-nanometer resolution. Science 272: 85-87.
[9] Kovacs G T A, Maluf N I, Petersen K E (1998) Bulk micromachining of silicon. Proceedings of the IEEE 86: 1536-1551.
[10] Bustillo J M, Howe R T, Muller R S (1998) Surface micromachining for microelectromechanical systems. Proceedings of the IEEE 86: 1552-1574.
[11] Boser B E, Howe R T (1996) Surface micromachined accelerometers. IEEE J. Solid-St. Circ. 31: 366-375.
[12] Takeuchi S, Suzuki T, Mabuchi K, Fujita H (2004) 3D flexible multichannel neural probe array. J. Micromech. Microeng. 14: 104.
[13] Fuller L F, Sudirgo S (2003) Bulk micromachined pressure sensor In: Proceedings of the 15th Biennial University/Government/Industry Microelectronics Symposium (IEEE, 2003), 317-320
[14] Honig R E, Woolston J R (1963) Laser-Induced Emission of Electrons, Ions, and Neutral Atoms from Solid Surfaces. Appl. Phys. Lett. 2: 138-139.
[15] Boot H A H, Clunie D M, Thorn R S A (1966) Micromachining with a pulsed gas laser. Electron. Lett. 2: 1.
[16] Anisimov S I (1968) Vaporization of Metal Absorbing Laser Radiation. Sov. Phys. JETP-USSR 27: 182-183.
[17] Kocher E, Tschudi L, Steffen J, Herziger G (1972) Dynamics of laser processing in transparent media IEEE J. Quantum Elec. QE 8: 120-&.
[18] Bourg H, Frederick R W (1975) Laser Machining of Silicon. J. Electrochem. Soc. 122: C260-C260.
[19] Longfell J (1971) High Speed Drilling in Alumina Substrates with a CO_2 Laser. Am Ceram Soc Bull 50: 251-&.
[20] McGuff P E, Deterling R A, Gottlieb L S, Bushnell D, Fahimi H D (1964) Surgical Applications of Laser. Ann. Surg. 160: 765-&.
[21] Cohen M I, Unger B A, Milkosky J F (1968) Laser Machining of Thin Films and Integrated Circuits. AT&T Tech. J. 47: 385-405.
[22] Steen W M (2003) Laser material processing. New York: Springer. 408 p.
[23] Ion J C (2005) Laser processing of engineering materials : principles, procedure and industrial application. Oxford: Elsevier/Butterworth-Heinemann. 556 p.
[24] Kogelnik H, Li T (1966) Laser Beams and Resonators. Appl. Opt. 5: 1550-1567.
[25] Stuart B, Feit M, Rubenchik A, Shore B, Perry M (1995) Laser-Induced Damage in Dielectrics with Nanosecond to Subpicosecond Pulses. Phys. Rev. Lett. 74: 2248-2251.
[26] Lan B, Hong M H, Ye K D, Wang Z B, Chong T C (2003) Laser microfabrication of glass substrates by pocket scanning. In: Miyamoto I, Ostendorf A, Sugioka K, Helvajian H,

editors. Fourth International Symposium on Laser Precision Microfabrication. pp. 133-136.

[27] Ben-Yakar A, Byer R L (2002) Femtosecond laser machining of fluidic microchannels for miniaturized bioanalytical systems. In: Sugioka K, Gower M C, Haglund R F, Pique A, Dubowski J J, Hoving W, editors. Photon Processing in Microelectronics and Photonics. pp. 212-217.

[28] Lane D W (1990) The optical properties and laser irradiation of some common glasses. J. Phys. D Appl. Phys. 23: 1727.

[29] Correa D S, Cardoso M R, Tribuzi V, Misoguti L, Mendonca C R (2012) Femtosecond Laser in Polymeric Materials: Microfabrication of Doped Structures and Micromachining. IEEE J. Sel. Top. Quantum Elec. 18: 176-186.

[30] Vora K, Kang S, Shukla S, Mazur E (2012) Fabrication of disconnected three-dimensional silver nanostructures in a polymer matrix. Appl. Phys. Lett. 100: 063120.

[31] Strickland D, Mourou G (1985) Compression of amplified chirped optical pulses. Opt. Commun. 56: 219-221.

[32] Diels J-C, Rudolph W (2006) Ultrashort laser pulse phenomena : fundamentals, techniques, and applications on a femtosecond time scale. Burlington, MA: Academic Press. 652 p.

[33] Sibbett W, Lagatsky A A, Brown C T A (2012) The development and application of femtosecond laser systems. Opt. Expr. 20: 6989-7001.

[34] Keller U (2010) Ultrafast solid-state laser oscillators: a success story for the last 20 years with no end in sight. Appl. Phys. B-Las. Opt. 100: 15-28.

[35] Russbueldt P, Mans T, Weitenberg J, Hoffmann H D, Poprawe R (2010) Compact diode-pumped 1.1 kW Yb:YAG Innoslab femtosecond amplifier. Opt. Lett. 35: 4169 -4171.

[36] Umhofer U, Jäger E, Bischoff C (2011) Refractive and diffractive laser beam shaping optics. Laser Technik Journal 8: 24-27.

[37] Bloembergen N (1974) Laser-induced electric breakdown in solids. IEEE J. Quantum Elec. QE10: 375-386.

[38] Du D, Liu X, Korn G, Squier J, Mourou G (1994) Laser-induced breakdown by impact ionization in $Si0_2$ with pulse widths from 7 ns to 150 fs. Appl. Phys. Lett. 64: 3071-3073.

[39] Reif J, Costache F (2006) Femtosecond laser interaction with solid surfaces: explosive ablation and self-assembly of ordered nanostructures. In: Rempe G, Scully M O, editors. Advances in Atomic Molecular, and Optical Physics, V. 53. San Diego: Elsevier Academic Press Inc. pp. 227-251.

[40] Stoian R, Rosenfeld A, Ashkenasi D, Hertel I V, Bulgakova N M, Campbell E E B (2002) Surface charging and impulsive ion ejection during ultrashort pulsed laser ablation. Phys. Rev. Lett. 88: 097603.

[41] Bulgakova N M, Stoian R, Rosenfeld A, Hertel I V, Marine W, Campbell E E B (2005) A general continuum approach to describe fast electronic transport in pulsed laser irradiated materials: The problem of Coulomb explosion. Appl. Phys. A-Mat. Sci. Proc. 81: 345-356.

[42] Kanavin A P, Smetanin I V, Isakov V A, Afanasiev Y V, Chichkov B N, Wellegehausen B, Nolte S, Momma C, Tunnermann A (1998) Heat transport in metals irradiated by ultrashort laser pulses. Phys. Rev. B 57: 14698-14703.

[43] Singh N (2004) Relaxation between electrons and surface phonons of a homogeneously photoexcited metal film. Pramana-J. Phys. 63: 1083-1087.

[44] Stuart B C, Feit M D, Herman S, Rubenchik A M, Shore B W, Perry M D (1996) Nanosecond-to-femtosecond laser-induced breakdown in dielectrics. Phys. Rev. B 53: 1749-1761.

[45] Lorazo P, Lewis L J, Meunier M (2003) Short-pulse laser ablation of solids: From phase explosion to fragmentation. Phys. Rev. Lett. 91: 225502.

[46] Perez D, Lewis L J (2003) Molecular-dynamics study of ablation of solids under femtosecond laser pulses. Phys. Rev. B 67: 184102.

[47] Zhigilei L V (2003) Dynamics of the plume formation and parameters of the ejected clusters in short-pulse laser ablation. Appl. Phys. A-Mat. Sci. Proc. 76: 339-350.

[48] Kautek W, Kruger J, Lenzner M, Sartania S, Spielmann C, Krausz F (1996) Laser ablation of dielectrics with pulse durations between 20 fs and 3 ps. Appl. Phys. Lett. 69: 3146-3148.

[49] Keldysh L V (1965) Ionization in the field of a strong electromagnetic wave. Sov. Phys. JETP-USSR 20: 1307-1314.

[50] Joglekar A P, Liu H, Spooner G J, Meyhofer E, Mourou G, Hunt A J (2003) A study of the deterministic character of optical damage by femtosecond laser pulses and applications to nanomachining. Appl. Phys. B-Las. Opt. 77: 25-30.

[51] Gamaly E G, Rode A V, Luther-Davies B, Tikhonchuk V T (2002) Ablation of solids by femtosecond lasers: ablation mechanism and ablation thresholds for metals and dielectrics. Phys. Plasmas 9: 949-957.

[52] Borghesi M, Romagnani L, Schiavi A, Campbell D H, Haines M G, Willi O, Mackinnon A J, Galimberti M, Gizzi L, Clarke R J, Hawkes S (2003) Measurement of highly transient electrical charging following high-intensity laser–solid interaction. Appl. Phys. Lett. 82: 1529.

[53] Born M, Wolf E (1999) Principles of optics : electromagnetic theory of propagation, interference and diffraction of light. New York: Cambridge University Press. 952 p.

[54] Hirayama Y, Obara M (2002) Heat effects of metals ablated with femtosecond laser pulses. Appl. Surf. Sci. 197: 741-745.

[55] Machado L M (to be published in 2012) Micromachining of optical components with femtosecond laser. Ph.D. Thesis (Universidade de São Paulo, São Paulo).

[56] Liu J M (1982) Simple technique for measurements of pulsed Gaussian-beam spot sizes. Opt. Lett. 7: 196-198.
[57] Samad R E, Vieira N D (2006) Geometrical method for determining the surface damage threshold for femtosecond laser pulses. Las. Phys. 16: 336-339.
[58] Samad R E, Baldochi S L, Vieira Jr N D (2008) Diagonal scan measurement of Cr:LiSAF 20 ps ablation threshold. Appl. Opt. 47: 920-924.
[59] Mero M, Clapp B, Jasapara J C, Rudolph W, Ristau D, Starke K, Kruger J, Martin S, Kautek W (2005) On the damage behavior of dielectric films when illuminated with multiple femtosecond laser pulses. Opt. Eng. 44: 051107.
[60] Costache F, Eckert S, Reif J (2008) Near-damage threshold femtosecond laser irradiation of dielectric surfaces: desorbed ion kinetics and defect dynamics. Appl. Phys. A-Mat. Sci. Proc. 92: 897-902.
[61] Courrol L C, Samad R E, Gomes L, Ranieri I M, Baldochi S L, de Freitas A Z, Vieira N D (2004) Color center production by femtosecond pulse laser irradiation in LiF crystals. Opt. Expr. 12: 288-293.
[62] Jee Y, Becker M F, Walser R M (1988) Laser-induced damage on single-crystal metal surfaces. J. Opt. Soc. Am. B 5: 648-659.
[63] Ashkenasi D, Lorenz M, Stoian R, Rosenfeld A (1999) Surface damage threshold and structuring of dielectrics using femtosecond laser pulses: the role of incubation. Appl. Surf. Sci. 150: 101-106.
[64] Martin S, Hertwig A, Lenzner M, Kruger J, Kautek W (2003) Spot-size dependence of the ablation threshold in dielectrics for femtosecond laser pulses. Appl. Phys. A-Mat. Sci. Proc. 77: 883-884.
[65] Lim Y C, Boukany P E, Farson D F, Lee L J (2011) Direct-write femtosecond laser ablation and DNA combing and imprinting for fabrication of a micro/nanofluidic device on an ethylene glycol dimethacrylate polymer. J. Micromech. Microeng. 21: 015012.
[66] Gomez D, Goenaga I (2006) On the incubation effect on two thermoplastics when irradiated with ultrashort laser pulses: Broadening effects when machining microchannels. Appl. Surf. Sci. 253: 2230-2236.
[67] Choi H W, Farson D F, Bovatsek J, Arai A, Ashkenasi D (2007) Direct-write patterning of indium-tin-oxide film by high pulse repetition frequency femtosecond laser ablation. Appl. Opt. 46: 5792-5799.
[68] Machado L M, Samad R E, de Rossi W, Vieira Junior N D (2012) D-Scan measurement of ablation threshold incubation effects for ultrashort laser pulses. Opt. Expr. 20: 4114-4123.
[69] Wolfram Research Inc. (retrieved 2012) Jacobi theta function J_3, http://functions.wolfram.com/EllipticFunctions/EllipticTheta3/06/01/03/.
[70] Reif J, Costache F, Varlamova O, Jia G, Ratzke M (2009) Self-organized regular surface patterning by pulsed laser ablation. Phys. Status Solidi C 6: 681-686.

[71] Mei H, Wang C, Yao J, Chang Y-C, Cheng J, Zhu Y, Yin S, Luo C (2011) Development of novel flexible black silicon. Opt. Commun. 284: 1072-1075.

[72] Halbwax M, Sarnet T, Delaporte P, Sentis A, Etienne H, Torregrosa F, Vervisch V, Perichaud I, Martinuzzi S (2008) Micro and nano-structuration of silicon by femtosecond laser: Application to silicon photovoltaic cells fabrication. Thin Solid Films 516: 6791-6795.

[73] Schlie S, Fadeeva E, Koroleva A, Ovsianikov A, Koch J, Ngezahayo A, Chichkov B N (2011) Laser-based nanoengineering of surface topographies for biomedical applications. Photonic. Nanostruct. 9: 159-162.

[74] Vorobyev A Y, Guo C (2007) Femtosecond laser structuring of titanium implants. Appl. Surf. Sci. 253: 7272-7280.

[75] Yasumaru N, Miyazaki K, Kiuchi J, Sentoku E (2011) Frictional properties of diamond-like carbon glassy carbon and nitrides with femtosecond-laser-induced nanostructure. Diam, Relat. Mater. 20: 542-545.

[76] Tang M, Hong M H, Choo Y S (2008) Hydrophobic Surface Fabrication by Laser Micropatterning. 779 p.

[77] Bizi-Bandoki P, Benayoun S, Valette S, Beaugiraud B, Audouard E (2011) Modifications of roughness and wettability properties of metals induced by femtosecond laser treatment. Appl. Surf. Sci. 257: 5213-5218.

[78] Vorobyev A Y, Guoa C (2008) Colorizing metals with femtosecond laser pulses. Appl. Phys. Lett. 92: 041914.

[79] Ahsan M S, Ahmed F, Kim Y G, Lee M S, Jun M B G (2011) Colorizing stainless steel surface by femtosecond laser induced micro/nano-structures. Appl. Surf. Sci. 257: 7771-7777.

[80] Mateo M P, Ctvrtnickova T, Fernandez E, Ramos J A, Yanez A, Nicolas G (2009) Laser cleaning of varnishes and contaminants on brass. Appl. Surf. Sci. 255: 5579-5583.

[81] Pouli P, Melessanaki K, Giakoumaki A, Argyropoulos V, Anglos D (2005) Measuring the thickness of protective coatings on historic metal objects using nanosecond and femtosecond laser induced breakdown spectroscopy depth profiling. Spectrochim. Acta B 60: 1163-1171.

[82] Dumitru G, Luscher B, Krack M, Bruneau S, Hermann J, Gerbig Y (2005) Laser processing of hardmetals: Physical basics and applications. Int. J. Refract. Met. H. 23: 278-286.

[83] Urech L, Lippert T, Wokaun A, Martin S, Madebach H, Kruger J (2006) Removal of doped poly(methylmetacrylate) from tungsten and titanium substrates by femto- and nanosecond laser cleaning. Appl. Surf. Sci. 252: 4754-4758.

[84] Hermann J, Benfarah M, Coustillier G, Bruneau S, Axente E, Guillemoles J F, Sentis M, Alloncle P, Itina T (2006) Selective ablation of thin films with short and ultrashort laser pulses. Appl. Surf. Sci. 252: 4814-4818.

[85] Atanasov P A, Takada H, Nedyalkov N N, Obara M (2007) Nanohole processing on silicon substrate by femtosecond laser pulse with localized surface plasmon polariton. Appl. Surf. Sci. 253: 8304-8308.

[86] Pronko P P, Dutta S K, Squier J, Rudd J V, Du D, Mourou G (1995) Machining of sub-micron holes using a femtosecond laser at 800 nm. Opt. Commun. 114: 106-110.

[87] Venkatakrishnan K, Tan B, Sivakumar N R (2002) Sub-micron ablation of metallic thin film by femtosecond pulse laser. Opt. Laser Technol. 34: 575-578.

[88] Lim C S, Hong M H, Lin Y, Chen G X, Kumar A S, Rahman M, Tan L S, Fuh J Y, Lim G C (2007) Sub-micron surface patterning by laser irradiation through microlens arrays. J. Mat. Process. Tech. 192: 328-333.

[89] Wang X C, Zheng H Y, Chu P L, Tan J L, Teh K M, Liu T, Ang B C Y, Tay G H (2010) Femtosecond laser drilling of alumina ceramic substrates. Appl. Phys. A-Mat. Sci. Proc. 101: 271-278.

[90] Li C, Lee S, Nikumb S (2009) Femtosecond Laser Drilling of Alumina Wafers. J. Electron. Mater. 38: 2006-2012.

[91] Wang Y, Dai N, Li Y, Wang X, Lu P (2007) Ablation and cutting of silicon wafer and micro-mold fabrication using femtosecond laser pulses. J. Laser Appl. 19: 240-244.

[92] Lee S, Yang D, Nikumb S (2008) Femtosecond laser micromilling of Si wafers. Appl. Surf. Sci. 254: 2996-3005.

[93] Suriano R, Kuznetsov A, Eaton S M, Kiyan R, Cerullo G, Osellame R, Chichkov B N, Levi M, Turri S (2011) Femtosecond laser ablation of polymeric substrates for the fabrication of microfluidic channels. Appl. Surf. Sci. 257: 6243-6250.

[94] van Brakel A, Grivas C, Petrovich M N, Richardson D J (2007) Micro-channels machined in microstructured optical fibers by femtosecond laser. Opt. Expr. 15: 8731-8736.

[95] Alemohammad H, Toyserkani E, Pinkerton A J (2008) Femtosecond laser micromachining of fibre Bragg gratings for simultaneous measurement of temperature and concentration of liquids. J. Phys. D Appl. Phys. 41: 185101.

[96] Lan X, Han Y, Wei T, Zhang Y, Jiang L, Tsai H-L, Xiao H (2009) Surface-enhanced Raman-scattering fiber probe fabricated by femtosecond laser. Opt. Lett. 34: 2285-2287.

[97] Said A A, Dugan M, de Man S, Iannuzzi D (2008) Carving fiber-top cantilevers with femtosecond laser micromachining. J. Micromech. Microeng. 18: 035005.

[98] Nolte S, Momma C, Jacobs H, Tunnermann A, Chichkov B N, Wellegehausen B, Welling H (1997) Ablation of metals by ultrashort laser pulses. J. Opt. Soc. Am. B 14: 2716-2722.

[99] Le Harzic R, Breitling D, Weikert M, Sommer S, Fohl C, Valette S, Donnet C, Audouard E, Dausinger F (2005) Pulse width and energy influence on laser micromachining of metals in a range of 100 fs to 5 ps. Appl. Surf. Sci. 249: 322-331.

[100] Ancona A, Doering S, Jauregui C, Roeser F, Limpert J, Nolte S, Tuennermann A (2009) Femtosecond and picosecond laser drilling of metals at high repetition rates and average powers. Opt. Lett. 34: 3304-3306.

[101] Doering S, Ancona A, Haedrich S, Limpert J, Nolte S, Tuennermann A (2010) Microdrilling of metals using femtosecond laser pulses and high average powers at 515 nm and 1030 nm. Appl. Phys. A-Mat. Sci. Proc. 100: 53-56.

[102] Schille J, Ebert R, Loeschner U, Scully P, Goddard N, Exner H (2010) High repetition rate femto second laser processing of metals. In: Heisterkamp A, Neev J, Nolte S, trebino R P, editors. Frontiers in Ultrafast Optics: Biomedical, Scientific, and Industrial Applications X.

[103] Zhang Q, Guo X P, Dai N L, Lu P X (2009) Corrosion and Fatigue Testing of Microsized 304 Stainless Steel Beams Fabricated by Femtosecond Laser. J. Mater. Sci. Technol. 25: 187-193.

[104] Momma C, Knop U, Nolte S (1999) Laser Cutting of Slotted Tube Coronary Stents – State-of-the-Art and Future Developments. Prog. Biom. Res. 4: 45-51.

[105] Li C D, Nikumb S, Wong F (2006) An optimal process of femtosecond laser cutting of NiTi shape memory alloy for fabrication of miniature devices. Opt. and Las. in Eng. 44: 1078-1087.

[106] Weck A, Crawford T H R, Wilkinson D S, Haugen H K, Preston J S (2008) Laser drilling of high aspect ratio holes in copper with femtosecond, picosecond and nanosecond pulses. Appl. Phys. A-Mat. Sci. Proc. 90: 537-543.

[107] Campbell B R, Palmer J A, Semak V V (2007) Peculiarity of metal drilling with a commercial femtosecond laser. Appl. Surf. Sci. 253: 6334-6338.

[108] Gamaly E G, Juodkazis S, Nishimura K, Misawa H, Luther-Davies B (2006) Laser-matter interaction in the bulk of a transparent solid: Confined microexplosion and void formation. Phys. Rev. B 73: 214101.

[109] Dubov M, Bennion I, Nikogosyan D N, Bolger P, Zayats A V (2008) Point-by-point inscription of 250 nm period structure in bulk fused silica by tightly focused femtosecond UV pulses. J. Opt. A: Pure Appl. Opt. 10: 025305.

[110] Ams M, Dekker P, Marshall G D, Withford M J (2009) Monolithic 100 mW Yb waveguide laser fabricated using the femtosecond-laser direct-write technique. Opt. Lett. 34: 247-249.

[111] Dharmadhikari J A, Dharmadhikari A K, Bhatnagar A, Mallik A, Singh P C, Dhaman R K, Chalapathi K, Mathur D (2011) Writing low-loss waveguides in borosilicate (BK7) glass with a low-repetition-rate femtosecond laser. Opt. Commun. 284: 630-634.

[112] Li C, Chen T, Si J, Chen F, Shi X, Hou X (2009) Fabrication of three-dimensional microchannels inside silicon using a femtosecond laser. J. Micromech. Microeng. 19:

[113] Machado L M, Samad R E, de Freitas A Z, Vieira Jr N D, de Rossi W (2011) Microchannels Direct Machining using the Femtosecond Smooth Ablation Method. Phys. Procedia 12: 67-75.

[114] Taylor R, Hnatovsky C, Simova E, Rayner D, Mehandale M, Bhardwaj V, Corkum P (2003) Ultra-high resolution index of refraction profiles of femtosecond laser modified silica structures. Opt. Expr. 11: 775-781.

[115] Saliminia A, Nguyen N T, Chin S L, Vallee R (2004) The influence of self-focusing and filamentation on refractive index modifications in fused silica using intense femtosecond pulses. Opt. Commun. 241: 529-538.